Cavity Expulsion and Weak Dewetting of Hydrophobic Solutes in Water

Gerhard Hummer and Shekhar Garde

Theoretical Division, MS K710, Los Alamos National Laboratory, Los Alamos, New Mexico 87545

(Received 15 October 1997)

Perturbation theory is used to study the solvation of nonpolar molecules in water, supported by extensive computer simulations. Two contributions to the solvent-mediated solute-water interactions are identified: a cavity potential of mean force that transforms by a simple translation when the solute size changes, and a solute-size-independent cavity-expulsion potential. The latter results in weak dewetting of the solute-water interface that can explain the approximate area dependence of solvation free energies with apparent surface tensions similar to macroscopic values. [S0031-9007(98)06064-5]

PACS numbers: 61.20.–p, 82.60.Lf, 87.15.Da, 87.15.Kg

Hydrophobic interactions play an important role in self-assembly phenomena in aqueous solutions, such as protein folding or the formation of membranes and micelles. Scaled-particle theory [1–3], Pratt-Chandler integral-equation theory [4], configurational entropy expansions [5], and recent theories based on cavity-size distributions [6–8] and density fluctuations [9] have greatly expanded our understanding of hydrophobic hydration on atomic length scales. However, the connection to mesoscopic and macroscopic phenomena remains largely unexplored. An exception is scaled-particle theory, which provides a basis for widely used phenomenological models parametrizing solvation free energies as proportional to surface areas.

The inhomogeneous structure of water in the vicinity of nonpolar solutes is the key to the thermodynamics of hydrophobic hydration. Here, we study the structure and thermodynamics of hydrophobic hydration using perturbation theory supported by extensive computer simulation data. Our ansatz for the solute-water oxygen radial distribution function (RDF) is

$$g_{sw}(r) = e^{-\beta u_{\rm rep}(r) - \beta\omega(r) + C(r)}, \tag{1}$$

where $\beta^{-1} = k_{\rm B}T$ with $k_{\rm B}$ the Boltzmann constant and T the temperature. The short-range repulsion $u_{\rm rep}(r)$ obtained from Weeks-Chandler-Anderson (WCA) [10] separation dominates $g_{sw}(r)$ at short distances,

$$u_{\rm rep}(r) = \begin{cases} u_{sw}(r) + \epsilon_{sw} & \text{for } r < 2^{1/6}\sigma_{sw}\,, \\ 0 & \text{otherwise}\,, \end{cases} \tag{2}$$

where the solute-water Lennard-Jones (LJ) interaction is $u_{sw}(r) = 4\epsilon_{sw}[(\sigma_{sw}/r)^{12} - (\sigma_{sw}/r)^{6}] = u_{\rm rep}(r) + u_{\rm att}(r)$. The renormalized potential $C(r)$ of the exponential (EXP) perturbation model [11,12] corrects for the weak attractions not considered in the WCA theory. In the limit of infinite solute dilution, $C(r)$ corresponds to the sum of the direct attraction $u_{\rm att}(r)$ and interactions transmitted by water molecules [12],

$$C(r) = -\beta u_{\rm att}(r) - \beta\rho_w u_{\rm att} * h_{ww}(r)\,. \tag{3}$$

ρ_w is the water density, and $h_{ww}(r) = g_{ww}(r) - 1$, where $g_{ww}(r)$ is the water-oxygen RDF. The asterisk indicates a three-dimensional convolution integral. Additional nontrivial contributions to $g_{sw}(r)$ are contained in $\omega(r)$.

In the perturbation model Eq. (1), the free-energy profile $-\beta^{-1}\ln g_{sw}(r)$ of a test water molecule as a function of the distance r from the solute can be separated into two terms: (1) $u_{\rm rep}(r) - \beta^{-1}C(r)$; and (2) $\omega(r)$. The former is identical to the ideal-gas result $u_{sw}(r)$ plus solvent-mediated attractive interactions $\rho_w u_{\rm att} * h_{ww}(r)$. The latter, $\omega(r)$, is approximately [and precisely so for $u_{\rm att}(r) = 0$] the free energy of bringing a test water molecule from infinity to a distance r from the solute when that water molecule does not interact directly with the solute but retains its interactions with other water molecules. This contribution is nontrivial; however, it is expected to be relatively insensitive to the details of the solute-water interactions for nonpolar solutes.

This insensitivity of $\omega(r)$ is indeed observed in extensive computer simulations of spherical LJ solutes of different sizes and attraction strengths in water [13]. For those solutes, the RDF's $g_{sw}(r)$ of water oxygens are almost identical after radial translation according to the peak position for solute diameters of less than about 0.5 nm (solute-solute LJ parameter σ_{ss}). This allows us to separate the solvent-induced solute-water interaction $\omega(r)$ into two contributions,

$$\omega(r) = \omega_0(r - r_0) + \Delta\omega(r - r_0)\,, \tag{4}$$

where the cavity potential of mean force (CPMF) $\omega_0(r - r_0)$ contains the solute-invariant part. Thus, solutes of different sizes and interactions with water have identical CPMF's $\omega_0(r - r_0)$ after translation by a distance r_0. The remaining size and interaction dependence is contained in $\Delta\omega(r - r_0)$. The radial shift r_0 for a given solute is chosen to be the distance where the solute-water repulsive force $-\partial u_{\rm rep}/\partial r$ equals 15 kJ/(mol nm). r_0 corresponds accurately to the peak position in the solute-water oxygen RDF's $g_{sw}(r)$ for small nonpolar solutes [16].

As shown in Fig. 1, the $\omega_0(r - r_0) + \Delta\omega(r - r_0)$ curves are indeed identical within statistical errors after translation by r_0, except for distances $r \lesssim r_0$. In that region, two effects compete: The solute volume becomes accessible to the test water molecule that does not

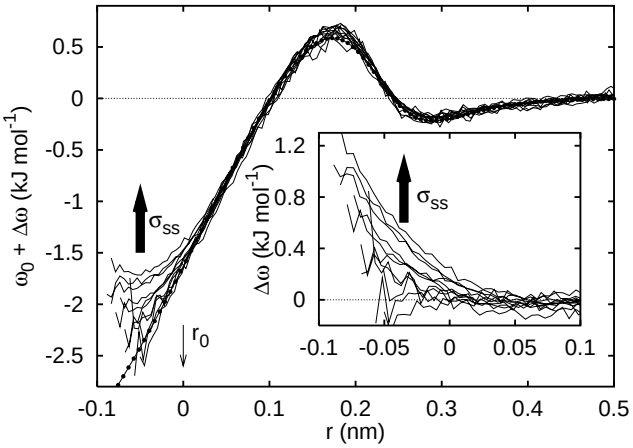

FIG. 1. Sum of CPMF and cavity-expulsion potential, $\omega_0(r) + \Delta\omega(r)$, from simulation RDF data for $\epsilon_{ss} = 1$ kJ/mol and $\sigma_{ss} = 0.2, 0.25, \ldots, 0.75$ nm. The $\omega_0(r)$ curve shown with filled circles was fitted to data for solute diameters $\sigma_{ss} = 0.2, 0.25, \ldots, 0.5$ nm and interaction strengths $\epsilon_{ss} = 0.1, 0.2, \ldots, 1.0$ kJ/mol. The inset shows the cavity-expulsion interaction $\Delta\omega(r)$. Thick arrows indicate trends with growing σ_{ss}. $r = 0$ corresponds to the approximate peak position r_0 of $g_{sw}(r)$.

interact with the solute, with the resulting free-energy gain contained in the solute-size-independent CPMF $\omega_0(r)$. However, the test water molecule also loses attractive interactions with the water phase, resulting in an effective "cavity-expulsion potential" $\Delta\omega(r)$ that depends on solute size. For small solutes, the cavity expulsion is negligible as the test water molecule retains sufficient interaction partners even at the center of the solute. For large solutes, however, the loss can amount to as much as the negative excess chemical potential $-\mu_0$ of water, corresponding to a transfer of the test water molecule from bulk liquid water into vacuum.

We find that $\Delta\omega(r)$ obtained from computer simulations can be approximated by a potential that is shifted according to the local curvature of the solute-water interface (see Fig. 1). Here, we use a form qualitatively suggested by the simulation data, $\Delta\omega(r) = -0.5\mu_0 \,\mathrm{erfc}[(r + \Delta r_c)/s]$, which is zero for $r \to \infty$ and $-\mu_0$ for $r \to -\infty$ (erfc is the complementary error function; $s = 0.135$ nm) [19]. For spherical solutes, the cavity expulsion is centered at $r_0 - \Delta r_c$, just inside the solute. Δr_c is approximated by a simple function of the curvature $1/r_0$, $\Delta r_c \approx 0.216$ nm $+$ 0.004 nm$/r_0^3$, with the coefficients obtained from a fit to the available data. Thus, for small spherical solutes (large curvature), the shift Δr_c is large and the cavity expulsion $\Delta\omega(r)$ is negligible in regions with appreciable water density. In contrast, for larger solutes (small curvature), the cavity expulsion results in weak dewetting of the solute that increases with increasing solute size. $\Delta\omega(r)$ curves from simulation data using $\epsilon_{ss} = 1$ kJ/mol are shown in the inset of Fig. 1. For a solute of diameter $\sigma_{ss} = 0.7$ nm, there is already an appreciable effect at $r = 0$ corresponding to the peak position.

Figure 2 shows solute-water oxygen RDF's for various solute LJ parameters. We observe excellent agreement between the RDF's calculated using the perturbation theory Eq. (1) and simulations. The bottom panel illustrates the effect of the cavity expulsion. For a small solute ($\sigma_{ss} = 0.4$ nm), the cavity expulsion has no appreciable effect on the RDF's; whereas for a larger solute ($\sigma_{ss} = 0.7$ nm), it results in an outward shift and depression of the first peak in the RDF [20].

We can readily use the RDF model Eq. (1) to study the thermodynamics of hydrophobic hydration. The derivative of the excess chemical potential μ of the solute with respect to σ_{ss} can be expressed as a canonical average of the derivative of the solute-water interaction energy u_{sw},

$$\left(\frac{\partial\mu}{\partial\sigma_{ss}}\right)_{V,T,\epsilon_{ss}} = \left\langle\frac{\partial u_{sw}}{\partial\sigma_{ss}}\right\rangle = 4\pi\rho_w\int_0^\infty dr\, r^2\, g_{sw}(r) \times 2\epsilon_{sw}\sigma_{sw}^{-1}\left[12\left(\frac{\sigma_{sw}}{r}\right)^{12} - 6\left(\frac{\sigma_{sw}}{r}\right)^{6}\right]. \quad (5)$$

Water orientational degrees of freedom have been integrated out exactly in Eq. (5). The derivative of the chemical potential with respect to σ_{ss} is shown in Fig. 3.

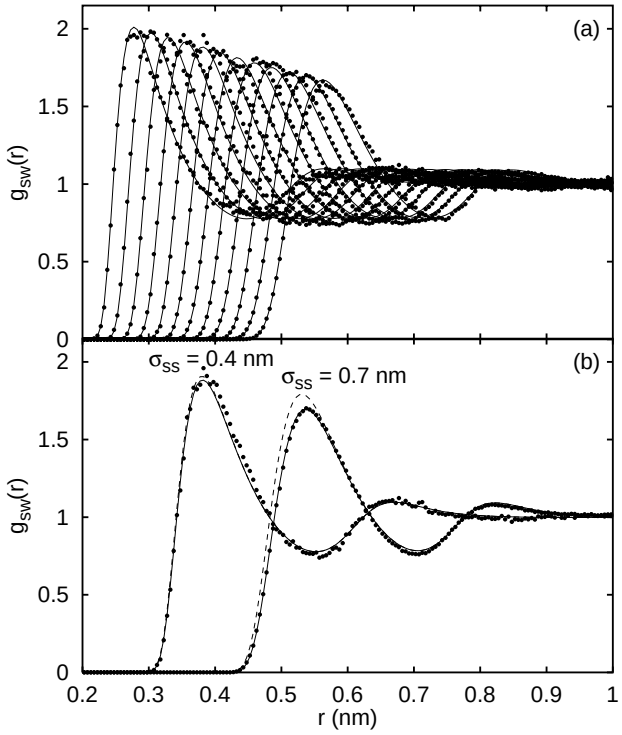

FIG. 2. Solute-water RDF's $g_{sw}(r)$. Simulation data are shown as filled circles (256 water molecules). Solid lines show the results of the perturbation theory Eq. (1). (a) Results for $\epsilon_{ss} = 1$ kJ/mol and $\sigma_{ss} = 0.2, 0.25, \ldots, 0.75, 0.75$ nm. For united-atom models of hydrocarbons [22], typical LJ parameters are $0.37 < \sigma_{ss} < 0.4$ nm and $0.5 < \epsilon_{ss} < 1.2$ kJ/mol. (b) Illustration of the effect of the cavity expulsion for $\sigma_{ss} = 0.4$ and 0.7 nm. The dashed line shows the result obtained from Eq. (1) without cavity expulsion [i.e., with $\Delta\omega(r) = 0$].

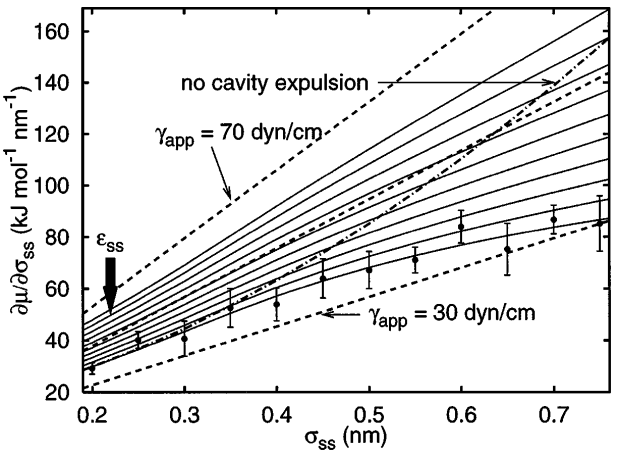

FIG. 3. Derivative of the excess chemical potential μ of LJ solutes with respect to the solute size σ_{ss}. Results are shown for $\epsilon_{ss} = 0.1, 0.2, \ldots, 1.0$ kJ/mol, where a thick arrow indicates the trend with growing ϵ_{ss}. The solid lines are calculated from the perturbation theory Eq. (1). For reference, simulation data are shown as filled circles for $\epsilon_{ss} =$ 1.0 kJ/mol, with error bars indicating one standard deviation estimated from block averages. The corresponding $\partial\mu/\partial\sigma_{ss}$ without cavity expulsion [$\Delta\omega(r) = 0$] is shown as a dot-dashed line. The results of surface-area models are shown as dashed lines, with apparent surface tensions $\gamma_{\text{app}} = 30$, 50, and 70 dyn/cm (1 dyn/cm = 10^{-3} N/m).

A comparison with data from simulations for $\epsilon_{ss} =$ 1.0 kJ/mol shows excellent agreement with the perturbation theory. The $\partial\mu/\partial\sigma_{ss}$ curves exhibit an approximately linear dependence on σ_{ss}. However, the slope depends on the LJ interaction strength ϵ_{ss}. Interestingly, the increase of $\partial\mu/\partial\sigma_{ss}$ with σ_{ss} is sublinear for large solutes with large ϵ_{ss} values. This could be a result of the increasing softness of water-solute LJ interactions with increasing σ_{ss} at constant ϵ_{ss}. The sublinear growth may also be an artifact of the approximate form used for the cavity-expulsion potential $\Delta\omega(r)$ [19].

Also included in Fig. 3 are chemical potentials calculated from phenomenological area laws, $\mu \approx \pi\sigma_{ss}^2\gamma_{\text{app}}$, for molecular surface areas $4\pi(\sigma_{ss}/2)^2$. We find that apparent surface tensions γ_{app} of about 40–60 dyn/cm best describe the data, in agreement with experimental surface tensions of 50 and 70 dyn/cm for water-alkane and water-vapor interfaces, respectively. However, we emphasize that using any single apparent surface tension results in considerable deviations from the observed chemical potentials when the solute size and attraction strength are varied within the range of $\sigma_{ss} \leq 0.7$ nm and $\epsilon_{ss} \leq 1$ kJ/mol considered here. Interestingly, the surface-area model for a water-alkane surface tension of 50 dyn/cm agrees precisely with the perturbation theory result for $\partial\mu/\partial\sigma_{ss}$ for LJ parameters $\sigma_{ss} = 0.3905$ nm and $\epsilon_{ss} = 0.494$ kJ/mol corresponding to an sp^3 CH_2 group of an *n*-alkane in the parametrization of Jorgensen *et al.* [22]. This may not be a pure coincidence, but suggests that cavity expulsion at macroscopic alkane-water interfaces acts according to the molecules forming the surface layer, rather than the alkane aggregate as a whole. In other words, a single large LJ solute is not a realistic representation of an alkane-water interface.

The effect of the cavity expulsion on the solvation thermodynamics is dramatic. Figure 3 shows the $\partial\mu/\partial\sigma_{ss}$ curve for $\epsilon_{ss} = 1$ kJ/mol calculated from Eq. (1) without cavity expulsion [$\Delta\omega(r) = 0$]. That curve shows a strong upturn, indicative of a large volume contribution to the solvation free energy. We conclude that the weak dewetting observed in Fig. 2(b) upon inclusion of $\Delta\omega(r)$ is sufficient to change the solvation thermodynamics qualitatively, bringing it into better agreement with phenomenological surface-area models.

We also calculated the apparent surface tensions of the entirely repulsive soft-sphere model $u_{sw}(r) = \beta^{-1}(\sigma_0/r)^{12}$ studied by Wallqvist and Berne [23]. For $0.645 \leq \sigma_0 \leq 0.725$ nm, we observe almost perfect area dependence with an apparent surface tension of about 83 dyn/cm. This value agrees well with the surface tension of 81 dyn/cm obtained upon correcting the explicit RER water simulation result of 108 dyn/cm [23] for different liquid-vapor surface tensions of SPC/E (75 dyn/cm) [24] and RER (100 dyn/cm) water models [23].

The cavity expulsion introduced here provides a first step towards reconciling the dewetting of large hard-sphere solutes proposed by Stillinger [1] with the simulation studies of soft interfaces [25], as well as large soft-sphere solutes [23]. Stillinger based his arguments for a vapor layer surrounding a large hard sphere immersed in water on the fact that the contact value of the RDF is small for liquid water, $g_{sw}(\sigma_{sw}^+) = \beta p/\rho \approx 2 \times 10^{-5}$. He also suggested that the water-vapor layer is wide on an atomic scale. The present theory favors weak dewetting with only a molecularly thin vapor layer surrounding nonpolar solutes. Interestingly, the maximum cavity-expulsion potential, $-\mu_0$, gives the correct magnitude for the contact value, $\exp(\beta\mu_0) \approx \beta p/\rho$. We note that several assumptions entering the present analysis warrant further examination: (1) We extrapolate the cavity expulsion observed for small solutes ($\sigma_{ss} \leq 0.75$ nm) to macroscopic hard walls using Eq. (1). (2) The hydration of hard spheres is assumed to be conceptually similar to that of soft spheres with weak attractions. (3) The cavity expulsion $\Delta\omega(r)$ is assumed to be independent of attractive interactions for $\beta\epsilon_{sw} \lesssim 1$.

The present theory explains the reduction in height and outward shift of the contact peak of the RDF's for large solutes [23] and of the water density distribution near a soft wall [25] [see Fig. 2(b)], without the presence of a dewetting regime. When we focus on concave surfaces or the region between two large hydrophobic solutes at short distance, such as the system studied recently by Wallqvist and Berne [23], complete dewetting in that region can be explained qualitatively. The energetic cost of transferring

a water molecule into a concave hydrophobic pocket is high, as that water molecule loses most of its interaction partners. This corresponds to a strong cavity-expulsion potential. The center of the cavity-expulsion potential can move *outside* a nonpolar solute of a *concave* shape, where concave is defined based on coarse-graining using a water molecule as the size parameter. In such a coarse-graining process, the narrow space between the two ellipsoids at short distance studied by Wallqvist and Berne [23] is *inside* the region where the cavity expulsion acts.

The nature of the cavity-expulsion potential also allows us to distinguish nonassociating liquids from water. For the extreme case of a hard-sphere fluid, the excess chemical potential in the bulk fluid is positive. This results in an effective "cavity attraction" that was indeed observed, with the contact value of the hard-sphere density at a wall being significantly higher than the contact value of the bulk RDF [26]. Cavity expulsion becomes relevant when attractive forces between solvent molecules gain importance. A density decrease at a wall resulting from increasing solvent-solvent attractions was, for instance, observed for dipolar hard spheres at a hard wall [27].

We must be cautious in applying cavity expulsion and weak dewetting to molecules or molecular assemblies such as proteins or micelles. The attractive interactions (van der Waals and electrostatic) with interior atoms effectively reduce the cavity expulsion of the surface layer. The tendency to dewet a nonpolar region on a protein surface is correspondingly less pronounced.

We are indebted to Dr. Lawrence R. Pratt, Dr. Angel E. García, Dr. Michael E. Paulaitis, and Dr. Henry S. Ashbaugh for many valuable discussions about hydrophobic hydration. This work was done under the auspices of the U.S. Department of Energy, supported through a Los Alamos National Laboratory LDRD grant.

[1] F. H. Stillinger, J. Solut. Chem. **2**, 141 (1973).
[2] H. Reiss, Adv. Chem. Phys. **9**, 1 (1965).
[3] R. A. Pierotti, Chem. Rev. **76**, 717 (1976).
[4] L. R. Pratt and D. Chandler, J. Chem. Phys. **67**, 3683 (1977).
[5] T. Lazaridis and M. E. Paulaitis, J. Phys. Chem. **96**, 3847 (1992).
[6] A. Pohorille and L. R. Pratt, J. Am. Chem. Soc. **112**, 5066 (1990).
[7] G. Hummer, S. Garde, A. E. García, A. Pohorille, and L. R. Pratt, Proc. Natl. Acad. Sci. U.S.A. **93**, 8951 (1996).
[8] S. Garde, G. Hummer, A. E. García, M. E. Paulaitis, and L. R. Pratt, Phys. Rev. Lett. **77**, 4966 (1996).
[9] D. Chandler, Phys. Rev. E **48**, 2898 (1993).
[10] J. D. Weeks, D. Chandler, and H. C. Andersen, J. Chem. Phys. **54**, 5237 (1971).
[11] H. C. Andersen and D. Chandler, J. Chem. Phys. **57**, 1918 (1972).
[12] L. R. Pratt and D. Chandler, J. Chem. Phys. **73**, 3434 (1980).
[13] All simulation results presented here are based on Monte Carlo calculations of systems with 128 or 256 SPC/E water molecules [14] and one LJ solute molecule. Ewald summation was used (see Ref. [15] for more details). Solute (σ_{ss}, ϵ_{ss}) and water LJ parameters ($\sigma_{ww} = 0.316\,556$ nm, $\epsilon_{ww} = 0.650\,170$ kJ/mol) are combined using Lorentz-Berthelot rules: $\sigma_{sw} = 0.5(\sigma_{ss} + \sigma_{ww})$ and $\epsilon_{sw} = (\epsilon_{ss}\epsilon_{ww})^{1/2}$. Simulations for small solutes ($\sigma_{ss} \leq 0.4$ nm) were performed in canonical ($T = 298$ K) ensembles with a constant total particle density of 33.33 nm^{-3}. For larger solutes, the volume was adjusted at the beginning of a simulation to give pressures within ± 100 bars.
[14] H. J. C. Berendsen, J. R. Grigera, and T. P. Straatsma, J. Phys. Chem. **91**, 6269 (1987).
[15] G. Hummer, L. R. Pratt, and A. E. García, J. Phys. Chem. **100**, 1206 (1996).
[16] For nonspherical nonpolar solutes, the inhomogeneous water density is determined almost entirely by the closest site of the solute [17,18]. This weak sensitivity of the water structure to the overall solute size and shape motivates a translationally invariant CPMF for nonspherical solute geometries as well.
[17] S. Garde, G. Hummer, A. E. García, L. R. Pratt, and M. E. Paulaitis, Phys. Rev. E **53**, R4310 (1996).
[18] H. S. Ashbaugh and M. E. Paulaitis, J. Phys. Chem. **100**, 1900 (1996).
[19] Preliminary calculations of $\Delta\omega(r)$ from simulations using perturbative methods indicate a softer inset for $r < r_0$, with the softness depending on the interfacial curvature.
[20] We note that the solute-water oxygen RDF for model LJ solutes with parameters representative of krypton are found in good agreement with recent extended x-ray absorption fine structure spectroscopy (EXAFS) data [21].
[21] A. Filipponi, D. T. Bowron, C. Lobban, and J. L. Finney, Phys. Rev. Lett. **79**, 1293 (1997).
[22] W. L. Jorgensen, J. D. Madura, and C. J. Swenson, J. Am. Chem. Soc. **106**, 6638 (1984).
[23] A. Wallqvist and B. J. Berne, J. Phys. Chem. **99**, 2885 (1995); **99**, 2893 (1995).
[24] J. Alejandre, D. J. Tildesley, and G. A. Chapela, J. Chem. Phys. **102**, 4574 (1995).
[25] C. Y. Lee, J. A. McCammon, and P. J. Rossky, J. Chem. Phys. **80**, 4448 (1984).
[26] I. K. Snook and D. Henderson, J. Chem. Phys. **68**, 2134 (1978).
[27] Z. X. Tang, L. E. Scriven, and H. T. Davis, J. Chem. Phys. **96**, 4639 (1992).